ACS APPLIED ELECTRONIC MATERIALS

pubs.acs.org/acsaelm

Article

Derivatives of 2-Pyridone Exhibiting Hot-Exciton TADF for Sky-Blue and White OLEDs

Iryna Danyliv, Khrystyna Ivaniuk, Yan Danyliv, Igor Helzhynskyy, Viktorija Andruleviciene, Dmytro Volyniuk, Pavlo Stakhira, Glib V. Baryshnikov,* and Juozas V. Grazulevicius*

Cite This: *ACS Appl. Electron. Mater.* 2023, 5, 4174–4186

Read Online

ACCESS | Metrics & More | Article Recommendations | Supporting Information

Downloaded via KAUNAS UNIV OF TECH on August 31, 2023 at 06:20:04 (UTC).
See https://pubs.acs.org/sharingguidelines for options on how to legitimately share published articles.

ABSTRACT: Development of emissive materials for utilization in organic light-emitting diodes (OLEDs) remains a highly relevant research field. One of the most important aspects in the development of efficient emitters for OLEDs is the efficiency of triplet-to-singlet exciton conversion. There are many concepts proposed for the transformation of triplet excitons to singlet excitons, among which thermally activated delayed fluorescence (TADF) is the most efficient and widespread. One of the variations of the TADF concept is the hot exciton approach according to which the process of exciton relaxation into the lowest energy electronic state (internal conversion as usual) is slower than intersystem crossing between high-lying singlets and triplets. In this paper, we present the donor−acceptor materials based on 2-pyridone acceptor coupled to the different donor moieties through the phenyl linker demonstrating good performance as components of sky-blue, green-yellow, and white OLEDs. Despite relatively low photoluminescence quantum yields, the compound containing 9,9-dimethyl-9,10-dihydroacridine donor demonstrated very good efficiency in sky-blue OLED with the single emissive layer, which showed an external quantum efficiency (EQE) of 3.7%. It also forms a green-yellow-emitting exciplex with 4,4′,4″-tris[phenyl(*m*-tolyl)amino]triphenylamine. The corresponding OLED showed an EQE of 6.9%. The white OLED combining both exciplex and single emitter layers demonstrated an EQE of 9.8% together with excellent current and power efficiencies of 16.1 cd A^{-1} and 6.9 lm W^{-1}, respectively. Quantum-chemical calculations together with the analysis of photoluminescence decay curves confirm the ability of all of the studied compounds to exhibit TADF through the hot exciton pathway, but the limiting factor reducing the efficiency of OLEDs is the low photoluminescence quantum yields caused mainly by nonradiative intersystem crossing dominating over the radiative fluorescence pathway.

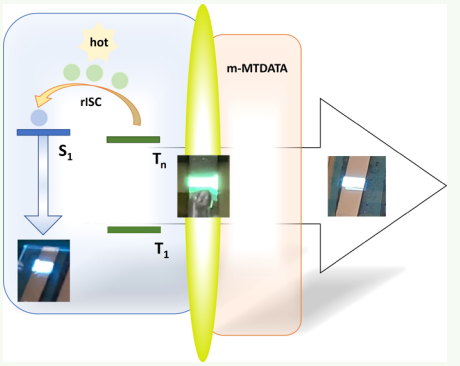

KEYWORDS: *pyridone, hot exciton, delayed fluorescence, exciplex, OLED*

1. INTRODUCTION

Rapid development of science and technology requires development of new organic materials and devices based on them as components of solid-state lighting and display technologies, medicine, biotechnology, etc. Considerable research interest in the development of new organic semiconductors for organic light-emitting devices (OLEDs) is related to the applications of these devices as components of flat panel displays, mobile electronics, smartphones, and lighting devices.[1−3] Despite the continuous efforts in the development of improved materials and devices, there is still room for their perfection.

A convenient way to improve device efficiency is the utilization of emitters exhibiting delayed fluorescence (DF). DF can be realized by the utilization of triplet excitons through the upconversion of nonradiative triplet states into radiative singlet states[4] in two ways. Two excited triplet states (T_1) during the upconversion process can produce one singlet (S_1) excited state. This process is named triplet−triplet annihilation (TTA). In another way, the temperature-assisted reverse intersystem crossing (RISC) process results in 100% efficiency of triplet state harvesting.[5] The process is known as thermally activated delayed fluorescence (TADF). The TADF mechanism appears by the conversion of harvested triplet excitons from the locally excited triplet state $T_{1(LE)}$ to the locally excited singlet state $S_{1(LE)}$ at the same spectral wavelength.[6] Small singlet−triplet energy splitting ($\Delta E_{S\text{-}T}$), spatial separation of highest occupied molecular orbital (HOMO)/lowest unoccupied molecular orbital (LUMO) with a small overlap, and efficient RISC process are the main requirements for the realization of the TADF mechanism.[7,8] RISC can occur not only between T_1 and S_1 but also between higher triplet (T_n, $n \geq 2$) and singlet states (S_m, $m \geq 1$).[9] Compounds allowing triplet harvesting via upper-level triplet−singlet RISC are used as emitters and hosts in the fabrication of

Received: April 4, 2023
Accepted: July 4, 2023
Published: July 21, 2023

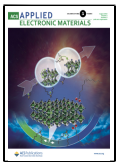

© 2023 The Authors. Published by American Chemical Society

Scheme 1. Synthetic Routes and Chemical Structures of Target Compounds

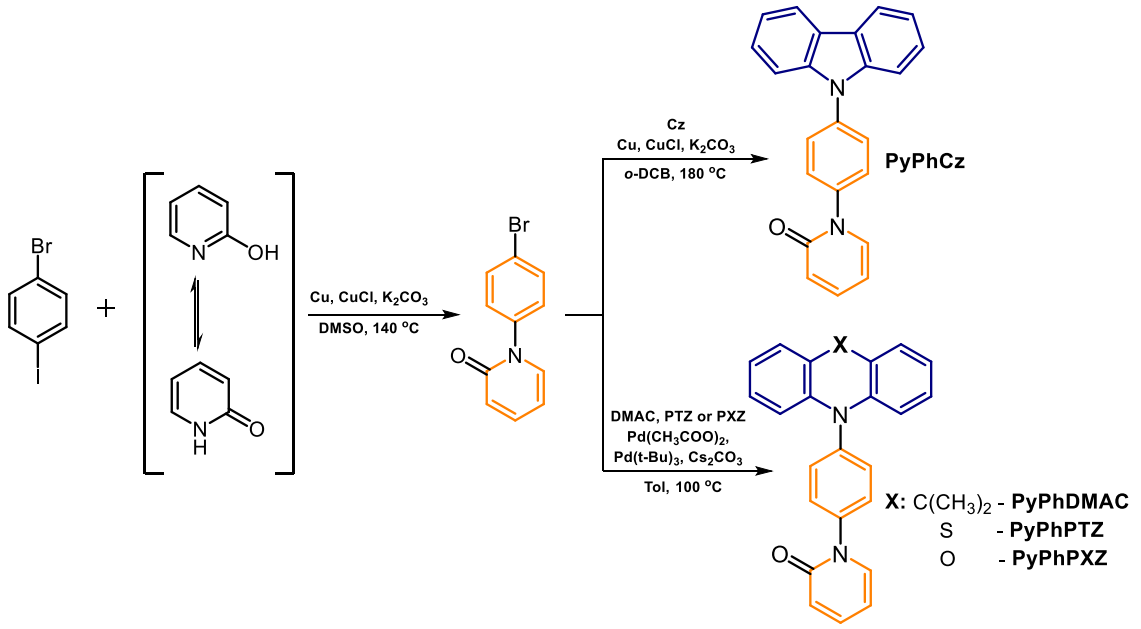

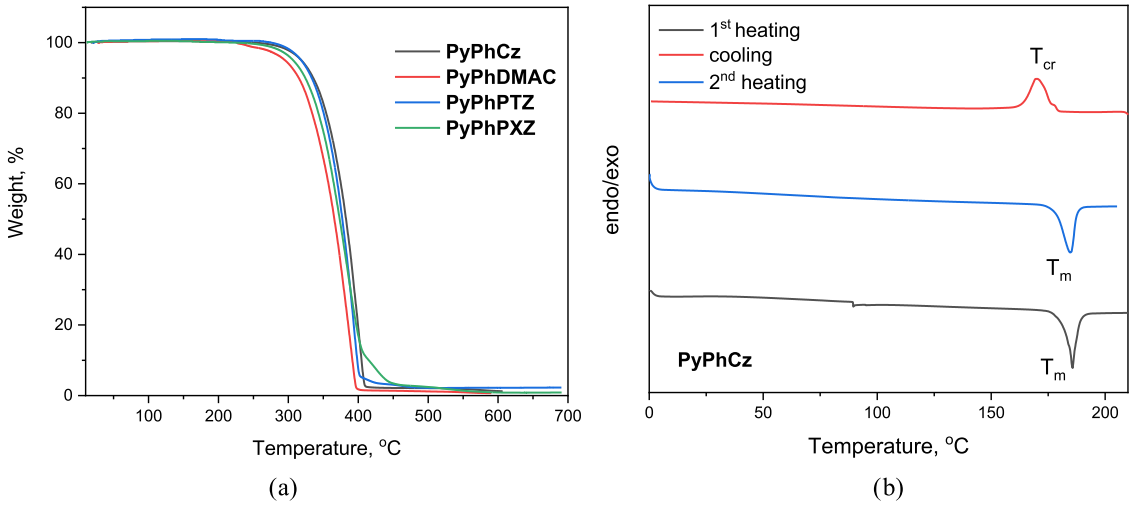

Figure 1. (a) TGA of the derivatives of 2-pyridone and (b) DSC curves of **PyPhCz**.

efficient host-free OLEDs with an external quantum efficiency (EQE) higher than 5%, which is the theoretical limit of EQE for electroluminescent devices based on emitters exhibiting prompt fluorescence.[10−13] Consequently, one of the ways of further enhancement of efficiency of the OLEDs is related to the development of novel compounds, including those exhibiting TADF, which occurs via upper-level triplet−singlet RISC.

Electron-donating nitrogen-containing aromatic heterocyclic compounds such as 9*H*-carbazole, 9,9-dimethyl-9,10-dihydroacridine, 9*H*-phenothiazine, 9*H*-phenoxazine, etc. have been widely used in the synthesis of efficient TADF emitters.[14−16] Their derivatives are characterized by high thermal and electrochemical stability, good hole-transporting properties, and high and stable triplet states.[17−19] In turn, electron-withdrawing moieties, such as nitrile,[20,21] triazine,[22,23] pyrimidine,[24,25] pyridine,[26] etc. were widely applied in the design of bipolar TADF emitters. For the achievement of TADF, careful selection of the combination of donor (D) and acceptor (A) moieties in the molecules is required.

In this article, we report the synthesis and characterization of new D−A-type TADF emitters based on a small acceptor (pyridin-2(1*H*)-one) moiety combined with a series of common donor species (9*H*-carbazole, 9,9-dimethyl-10*H*-acridane, 9*H*-phenothiazine, and 9*H*-phenoxazine). The compound containing 9,9-dimethyl-10*H*-acridane moiety, which exhibited the highest photoluminescence quantum yield in the solid state, was tested in electroluminescent devices. The EQE values of 3.7, 6.9, and 9.8% were achieved for sky-blue OLED with the single emissive layer, for green-yellow OLED based on the emission of exciplex with 4,4′,4″-tris[phenyl(*m*-tolyl)amino]triphenylamine (MTDATA), and for white OLED based on the combination of both exciplex and single layer emissions, respectively. In addition, this compound demonstrated the effect of "hot" exciton TADF.[9]

2. RESULTS AND DISCUSSION

2.1. Molecular Design and Synthesis. It is well known that 2-hydroxypyridine is capable of exhibiting keto−enol

https://doi.org/10.1021/acsaelm.3c00443
ACS Appl. Electron. Mater. 2023, 5, 4174−4186

tautomerization under specific conditions.[27] Utilization of this property makes it possible to implement two consequent amination reactions, which are depicted in Scheme 1. 9*H*-Carbazole, 9,9-dimethyl-9,10-dihydroacridine, 9*H*-phenothiazine, and 9*H*-phenoxazine were selected for the molecular design of the target compounds. The first step in the synthesis was Ullmann condensation, which afforded 2-pyridone substituted with a bromophenyl moiety. The following Ullmann condensation (in case of 9*H*-carbazole aromatic amine) or Buchwald−Hartwig cross-coupling reaction (in case of 9,9-dimethyl-9,10-dihydroacridine, 9*H*-phenothiazine and 9*H*-phenoxazine aromatic amines) yielded the target compounds 1-(4-(9*H*-carbazol-9-yl)phenyl)pyridin-2(1*H*)-one (**PyPhCz**), 1-(4-(9,9-dimethylacridin-10(9*H*)-yl)phenyl)pyridin-2(1*H*)-one (**PyPhDMAC**), 1-(4-(10*H*-phenothiazin-10-yl)phenyl)-pyridin-2(1*H*)-one (**PyPhPTZ**), and 1-(4-(10*H*-phenoxazin-10-yl)phenyl)pyridin-2(1*H*)-one (**PyPhPXZ**). The chemical structures of the obtained derivatives were confirmed by ^{1}H and ^{13}C NMR spectroscopy, mass spectrometry, and elemental analysis (Supporting Information).

2.2. Thermal Characterization. The thermal properties of the synthesized compounds were investigated by thermogravimetric analysis (TGA) and differential scanning calorimetry (DSC). TGA and DSC curves are shown in Figures 1a,b and S1. The temperatures of the transitions are summarized in Table 1.

Table 1. Thermal Characteristics of the Derivatives of 2-Pyridone

compound	T_{ID}[a], °C	T_m[b], °C	T_{cr}[c], °C	T_g[d], °C
PyPhCz	320	185	170	–
PyPhDMAC	295	247	167	–
PyPhPTZ	318	206	–	66
PyPhPXZ	307	175	–	66

[a]Determined by TGA; determined by DSC from. [b]First heating scan. [c]Cooling. [d]Second heating scan.

All derivatives exhibited a relatively high temperature of 5% weight loss (T_{ID}) ranging from 295 to 320 °C. The single-stage TGA curves reflecting full weight loss show that most of the compounds are subjected to sublimation during TGA measurements. The 2-pyridone derivatives were obtained as crystalline substances after synthesis and purification. Therefore, the endothermic melting peaks were observed for all of the derivatives in the first DSC heating scans (Figures 1b and S1). In the following cooling scans, compounds **PyPhCz** and **PyPhDMAC** showed crystallization signals at 170 and 167 °C, respectively. The melting signals were observed in the subsequent heating scans at 185 and 247 °C (Figures 1b and S1, Table 1). Meanwhile, compounds **PyPhPTZ** and **PyPhPXZ** were found to be able to form molecular glasses with glass-transition temperatures (T_g) of >66 °C (Figure S1 and Table 1).

2.3. Photophysical Properties. Before the investigation of the photophysical properties of the target compounds, UV−vis absorption and photoluminescence (PL) spectra of the tetrahydrofuran (THF) solution of acceptor 1-(4-bromophenyl)pyridin-2(1*H*)-one (BrPh2PY) were recorded (Figure 2a). In addition, PL and phosphorescence (phosphorus) spectra of the THF solution of BrPh2PY were recorded at 77 K (Figure 2b). The low-energy absorption band of the dilute THF solution of BrPh2PY peaked at 312 and 322 nm. The PL spectrum of BrPh2PY has a maximum at 379 nm. The relatively high lowest singlet (S_1 = 3.74 eV) and triplet (T_1 = 3.31 eV) energy levels were obtained for the selected acceptor (BrPh2PY). Typically, electron-accepting and electron-donating moieties with high triplet levels are utilized in the design of efficient TADF emitters.[28] Analysis of the photophysical properties of BrPh2PY shows that it has great potential to be used in the design of TADF emitters with different emission colors, including deep-blue color.

UV−vis absorption and photoluminescence (PL) spectra of the solutions of the derivatives of 2-pyridone in the solvents of the different polarities and of the solid films are shown in Figure 2c,d. The wavelengths of low-energy absorption and PL maxima are collected in Table 2. The low-energy absorption bands of the dilute solutions were observed in the region of 287−340 nm. Taking into account the absorption spectrum of BrPh2PY, it can be presumed that the low-energy absorption bands of the studied derivatives of 2-pyridone (**PyPhs**) result from their donor−acceptor structure. At wavelengths longer than 350 nm, absorption spectra of **PyPhs** are characterized by shoulders with long tails reaching 400 nm. These tails are caused by the intramolecular charge-transfer (CT) states formed by the donor−acceptor interactions in the ground state. The low-energy absorption bands of the solid films were found to be slightly bathochromically shifted (304−380 nm) in comparison with those of the corresponding solutions of the derivatives. The shifts are probably caused by the intermolecular interactions in the solid state.

The solutions in toluene and thin films of 2-pyridone derivatives demonstrated PL in the violet-blue range of the visible spectrum with emission intensity maxima in the regions of 399−472 and 411−480 nm, respectively. The bathochromic shifts of emission bands were observed for the THF solutions relative to those of the toluene solutions of the derivatives, with the wavelength maximum emission intensities varying from 407 to 550 nm (Table 2). PL and phosphorescence spectra were recorded at 77 K (Figure 2d). The lowest singlet (S_1) and triplet (T_1) energy levels and ΔE_{ST} values were determined from the high-energy onsets of the corresponding spectra (Table 2). Large ΔE_{ST} values for **PyPhs** (>0.39 eV) do not support the possibility of the reverse intersystem crossing between the lowest triplet and singlet states. The photoluminescence efficiencies were found to be rather low for both, toluene solutions and solid films. The highest photoluminescence quantum yields (PLQY) were observed for the solid sample of **PyPhDMAC** and for a toluene solution of **PyPhPXZ**. Taking into account these observations, we decided to focus on compound **PyPhDMAC** as an emissive component of OLEDs. Surprisingly, **PyPhDMAC**-based **OLED** demonstrated a quite high EQE of 3.7% (more details are given in the next section), which is close to the theoretical limit of 5% for fluorescent OLEDs. We assume that compound **PyPhDMAC** might exhibit TADF. As follows from our quantum-chemical calculations, **PyPhDMAC** sustains a three-state model (Tables 3 and 4) typical for emitters demonstrating TADF of type I through the spin−vibronic coupling mechanism (following nomenclature by Monkman and coauthors).[29] One should note that the S_1 state of **PyPhDMAC** can be assigned to the charge-transfer (^{1}CT) state (HOMO is localized on the donor part, while LUMO is on the acceptor part, Figure S2), while the T_1 state is localized on the acceptor part only (i.e., is the ^{3}LE state). Thus, spin−orbit coupling matrix element (SOCME) between these states is considerable (0.64 cm^{-1}, Table 4) in line with earlier reported conclusions by Brédas et al.[30] and is also consistent with the classical El-Sayed rule for ISC rates. The electronic config-

https://doi.org/10.1021/acsaelm.3c00443
ACS Appl. Electron. Mater. 2023, 5, 4174−4186

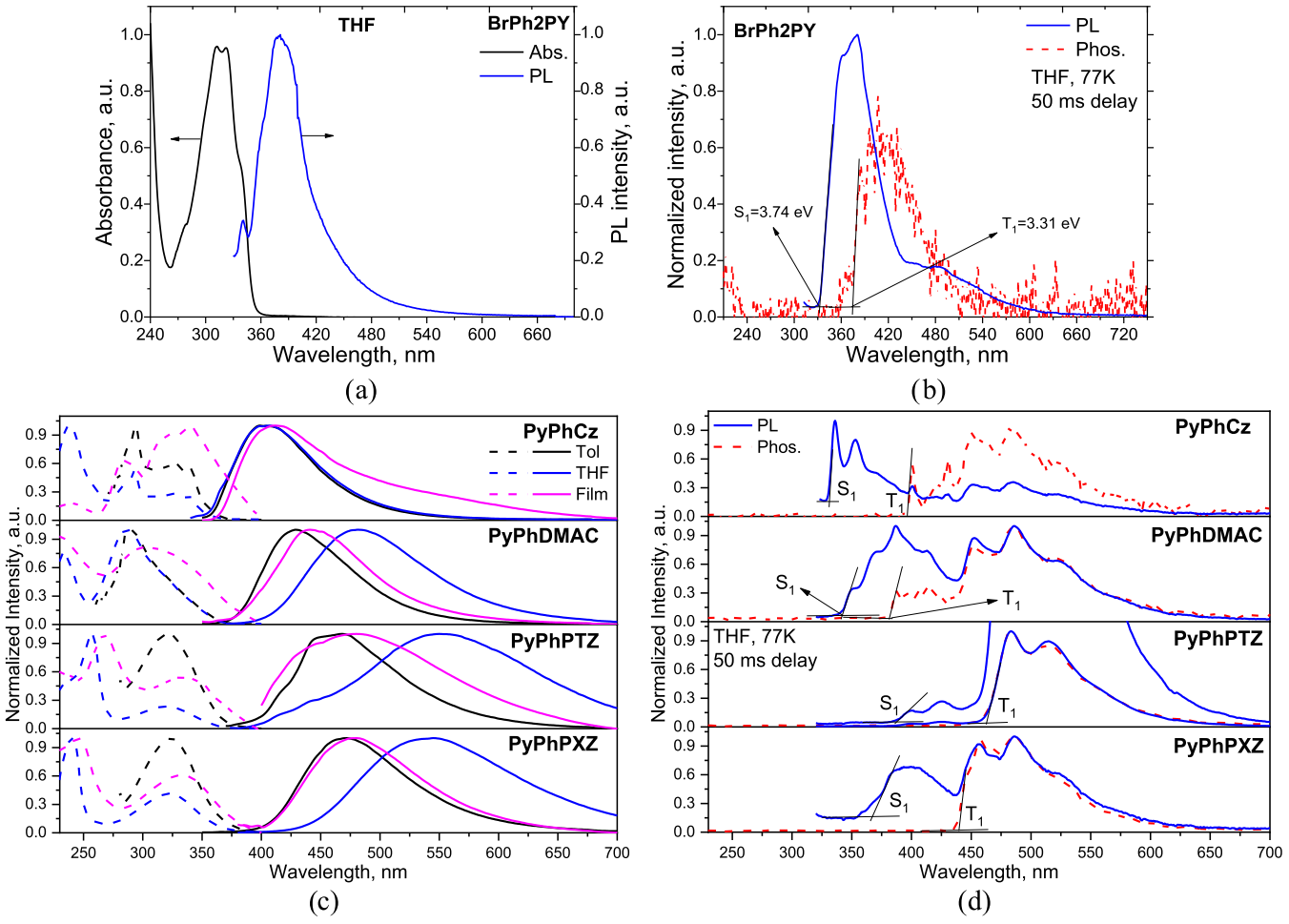

Figure 2. Absorption and PL spectra (a) as well as PL and Phos. spectra (b) of the dilute THF solution of BrPh2PY recorded at 77 K. Absorption (dashed lines) and PL (solid lines) spectra (c) of the toluene (Tol) and THF solutions as well as of solid films (Film) of the derivatives of 2-pyridone and PL and Phos. spectra (d) of their dilute THF solutions recorded at 77 K.

Table 2. Photophysical Characteristics of the Compounds

compound	λ_{abs} [a,b,c], nm	λ_{PL} [a,b,c], nm	Φ_{PL} [a]	Φ_{PL} [b]	Φ_{PL} [c]	S_1, eV	T_1, eV	ΔE_{ST}, eV
PyPhCz	340/340/380	399/407/411	0.04	0.02	0.02	3.77	3.12	0.65
PyPhDMAC	290/287/304	429/482/441	0.05	0.045	0.04	3.63	3.24	0.39
28PyPhPTZ	322/319/336	468/550/480	0.01	0.01	<0.01	3.19	2.67	0.52
PyPhPXZ	324/322/333	472/545/480	0.07	0.03	<0.01	3.38	2.82	0.56

[a]Toluene solution. [b]THF solution. [c]Solid state. λ_{abs} is the wavelength of absorption maximum; λ_{PL} is the wavelength of photoluminescence maximum; Φ is photoluminescence quantum yield. The concentration of solutions was 10^{-5} M.

uration of the T_2 state is the same as for the S_1 state (i.e., T_2 is the ^{3}CT state), and thus it is quasi-degenerated with ^{1}CT. Therefore, the mechanism of TADF exhibited by **PyPhDMAC** can be considered since ^{3}LE is coupled with ^{3}CT by vibronic coupling and ^{3}CT-to-^{1}CT rISC is thus possible (SOCME is small, 0.04 cm^{-1}, but nonzero). However, based on the T_1 state geometry of **PyPhDMAC**, our calculations predict very large S_1-T_1 (1.12 eV) and T_2-T_1 (1.11 eV) gaps that unbales efficient reverse internal conversion between ^{3}LE and ^{3}CT states. Thus, vibronically assisted TADF is not the case for **PyPhDMAC**. Another idea of how TADF can be realized in **PyPhDMAC** is the hot exciton concept.[9] Accounting for the fact that S_1 and T_2 states are quasi-degenerated and both correspond to HOMO−LUMO electronic configuration, the corresponding ^{3}CT (T_2) and ^{1}CT (S_1) excitons can be populated initially through electron−hole recombination (OLED is fabricated following the closest energy matching between injected electrons and holes vs LUMO and HOMO energy levels, respectively). Taking into account the very large T_2−T_1 separation, the internal conversion from T_2 to T_1 should be slower than T_2−S_1 reverse ISC (S_1−T_2 gap is only 0.01 eV, SOCME is small but nonzero, 0.04 cm^{-1}), which converts T_2 excitons to emissive S_1 excitons. Thus, the TADF channel for T_2 "hot" excitons should dominate over nonradiative quenching of T_2 excitons, which results in the OLED heterostructure demonstrating an external quantum efficiency of around 3.7%. For compound **PyPhCz**, four triplet states are lower in energy than the S_1 state, which makes a triplet yield high and thus quenches the S_1 state fluorescence. The rISC channel for compound **PyPhCz** is also possibly accounting for the close-lying T_4 and S_1 states of the same HOMO−LUMO configuration coupled by SOC with $\langle S_1|\hat{\mathbf{H}}_{SO}|T_n\rangle = 0.20$ cm^{-1} (at T_1 geometry). Also the T_5−S_2 channel is a possible way to get

https://doi.org/10.1021/acsaelm.3c00443
ACS Appl. Electron. Mater. 2023, 5, 4174−4186

Table 3. Excited State Energies for the Derivatives of 2-Pyridone[a]

compound	$E(S_1)$vert	$E(S_1)^{S1}$	$E(T_n)^{S1}$	$E(T_1)$vert	$E(S_1)^{T1}$	$E(T_n)^{T1}$
PyPhCz	3.77 (0.36) [3.65]	3.28 (0.38) [3.11]	2.30 (n = 1)	2.73	3.67	2.59 (n = 1)
			3.00 (n = 2)			2.73 (n = 2)
			3.24 (n = 3)			3.07 (n = 3)
						3.43 (n = 4)
PyPhDMAC	3.36 (10^{-4})	2.92 (10^{-3}) [2.89]	2.30 (n = 1)	2.73	3.11	1.99 (n = 1)
			2.91 (n = 2)			3.10 (n = 2)
PyPhPTZ	3.41 (5×10^{-4})	2.654 (4×10^{-4}) [2.65]	2.29 (n = 1)	2.73	2.58	1.94 (n = 1)
			2.41 (n = 2)			2.73 (n = 2)
			2.648 (n = 3)			2.98 (n = 3)
PyPhPXZ	3.09 (2×10^{-4})	2.579 (4×10^{-4}) [2.63]	2.30 (n = 1)	2.73	2.84	1.99 (n = 1)
			2.54 (n = 2)			2.77 (n = 2)
			2.577 (n = 3)			2.82 (n = 3)

[a]Calculated by the TDDFT/LC-ωPBE/6-31G(d) method (ω = 0.14; PCM model was used for accounting of toluene solvent effect). Experimental references are presented in parentheses.

Table 4. Orbital Nature of Low-Lying Excited States for the Derivatives of 2-Pyridone Together with the Values of Spin−Orbit Coupling Matrix Elements (SOCMEs) $\langle S_1|\hat{H}_{SO}|T_n\rangle$ Calculated at S_1 and T_1 State Geometries

compound	$\langle S_1\|\hat{H}_{SO}\|T_n\rangle^{S1}$, cm^{-1}	$\langle S_1\|\hat{H}_{SO}\|T_n\rangle^{T1}$, cm^{-1}	assignment^{S1}	assignment^{T1}
PyPhCz	0.30 (n = 1)	0.04 (n = 1)	S_1: H → L (96%)	S_1: H → L (89%)
	0.75 (n = 2)	0.53 (n = 2)	T_1: H-2 → L (78%)	T_1: H → L+1 (73%)
	0.30 (n = 3)	0.08 (n = 3)	T_2: H → L (61%)	T_2: H-2 → L (72%)
		0.20 (n = 4)	T_3: H-1 → L (88%)	T_3: H-1 → L+1 (72%)
				T_4: H → L (65%)
PyPhDMAC	0.93 (n = 1)	0.64 (n = 1)	S_1: H → L (97%)	S_1: H → L (97%)
	0.10 (n = 2)	0.04 (n = 2)	T_1: H-1 → L (86%)	T_1: H-1 → L (90%)
			T_2: H → L (97%)	T_2: H → L (96%)
PyPhPTZ	0.69 (n = 1)	3.21 (n = 1)	S_1: H → L (98%)	S_1: H → L+1 (93%)
	1.22 (n = 2)	1.75 (n = 2)	T_1: H-1 → L (75%)	S_2: H → L (70%)
	0.10 (n = 3)	2.96 (n = 3)	T_2: H → L+1 (69%)	T_1: H → L+1 (88%)
			T_3: H → L (95%)	T_2: H-1 → L (62%)
				T_3: H → L (68%)
PyPhPXZ	0.75 (n = 1)	0.58 (n = 1)	S_1: H → L (98%)	S_1: H → L (97%)
	1.35 (n = 2)	1.39 (n = 2)	T_1: H-1 → L (85%)	T_1: H-1 → L (90%)
	0.13 (n = 3)	0.09 (n = 3)	T_2: H → L+3 (49%)	T_2: H → L+3 (58%)
			T_3: H → L (94%)	T_3: H → L (96%)

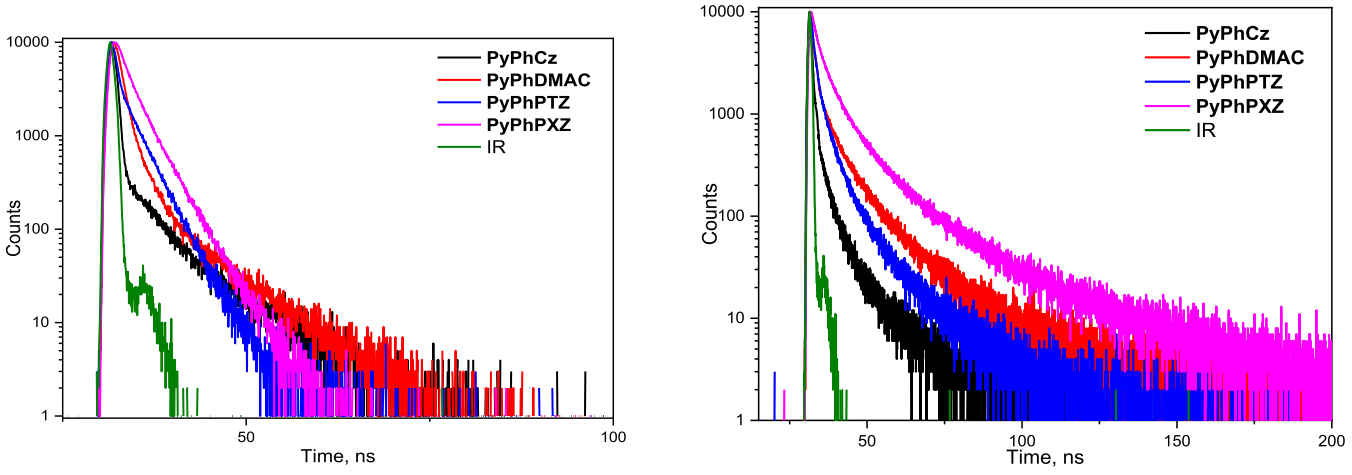

Figure 3. PL decay curves of the toluene solutions (left) and thin solid films (right) of the compounds recorded at room temperature.

rISC in **PyPhCz**. The gap is less than 0.1 eV, and the SOCME is 0.23 cm^{-1}.

Similarly, compound **PyPhPTZ** can show TADF through the rISC between hot excitons, mainly within the T_2−S_1 and T_3−S_2 pairs. It is important to note that the T_2−S_1 rISC channel is thermodynamically allowed (T_2 is higher in energy than S_1 by 0.15 eV; thus, it does not require thermal activation). At the same time, the gaps T_2−T_1 and T_3−T_1 are relatively large (0.79 and 1.04 eV, respectively), preventing internal conversion within these pairs. For the related compound **PyPhPXZ**, the hot

https://doi.org/10.1021/acsaelm.3c00443
ACS Appl. Electron. Mater. 2023, 5, 4174−4186

Table 5. Fitting Results for PL Decay Curves of the Toluene Solutions and Thin Solid Films of the 2-Pyridone Derivatives at Room Temperature

	toluene			films		
compound	τ_1, ns/Rel$_1$, %[a]	τ_2, ns/Rel$_2$, %[a]	χ^2	τ_1, ns/Rel$_1$, %[a]	τ_2, ns/Rel$_2$, %[a]	χ^2
PyPhCz	0.42/94.76	6.75/5.24	1.279	0.55/97.15	7.57/2.85	1.293
PyPhDMAC	1.03/89.43	6.56/10.57	1.286	1.05/57.61	6.35/42.39	1.125
PyPhPTZ	0.35/42.50	2.65/57.50	1.151	0.57/95.71	6.54/4.29	1.278
PyPhPXZ	1.37/42.37	3.16/57.63	1.085	0.58/90.90	7.95/9.10	1.240

[a]Rel$_1$ and Rel$_2$ (in %) are contribution ratios of lifetimes τ_1 and τ_2, respectively

exciton rISC mechanism is similar to that of **PyPhDMAC**, but an additional T_2 state is very close energetically to S_1 (0.07 eV lower) and T_3 (0.05 eV lower) states. This makes possible equilibration and mixing between T_2 and T_3 states through vibronic coupling, thus facilitating the rISC process. Similarly to **PyPhPTZ** and **PyPhDMAC**, the T_1 state is very low-lying for **PyPhPXZ**. This allows us to predict slow T_2-T_1 and T_3-T_1 nonradiative deactivations. Summarizing, all of the studied compounds may be able to exhibit TADF through the rISC involving hot excitons, but deactivation of the S_1 state through the ISC still dominates over the radiative decay of the S_1 state. This results in low quantum yields of photoluminescence (PLQYs of the solid samples of **PyPhPXZ** and **PyPhPTZ** are less than 1%, PLQY of the layer of **PyPhCz** is just 2% and that of the layer **PyPhDMAC** is 4%). This, to a great extent, limits the applicability of the synthesized compounds for the preparation of active layers of OLEDs. Modification of the linking group and chemical tuning of donor moieties can be considered as potential ways to enhance radiative rate constants.

Both the solutions and the solid samples of the compounds demonstrate similar trends of PL decay (Figure 3). The common trend for all of the cases is the presence of a very fast decay component in the range of 0.35−1.37 ns (Table 5). Accounting for the very weak fluorescence quantum yield observed for all of the compounds, this fast component can be assigned to nonradiative quenching of the S_1 state most likely through the ISC channel. Indeed, for the S-containing compound **PyPhPTZ** sustaining internal heavy atom effect on the ISC process, fast decay component (τ_1) is the fastest one in the whole series (just 0.34 ns for the solution in toluene). The second slower component of PL decay can be assigned to combined deactivation channels including ISC between S_1 and particular low-lying T_n states, prompt fluorescence, and TADF via a hot exciton channel. For example, one can assume that for **PyPhPXZ**, the toluene solution of which demonstrates the highest PLQY, τ_2 corresponds to a large amount of prompt fluorescence combined with S_1-T_2 and S_1-T_1 ISC, but in the case of **PyPhPTZ**, τ_2 lifetime corresponds mainly to S_1-T_2 and S_1-T_1 ISC accounting for negligible PLQY (Table 2).

For the solid films, both τ_1 and τ_2 are generally lower than for toluene and the contribution of τ_1 significantly dominates over τ_2 (Table 5). Only for **PyPhDMAC**, the contribution of τ_2 is equivalent to that of τ_1. This observation we interpret in terms of hot exciton TADF combined with prompt fluorescence in line with conclusions by Kuehne[31] and Ma[9,10] that upper-level rISC in hot exciton TADF materials is fast and practically indistinguishable from fluorescence. In summary, the results of photoluminescence decay measurements confirm the presence of hot exciton TADF of **PyPhDMAC** and explain the unusually high efficiency of the corresponding sky-blue OLED.

2.4. Electrochemical and Photoelectrical Properties. Cyclic voltammetry (CV) measurements were used to estimate the ionization potentials (IP$_{CV}$) and electron affinities (EA$_{CV}$), which are the key parameters of the materials used for the fabrication of the OLEDs (Table 6). CV curves of the solutions of the compounds in anhydrous dimethylformamide (DMF) are shown in Figure 4. The positive and negative voltages were applied for the investigation of the redox behavior of the synthesized compounds and the estimation of the electronic energy levels. Due to the observation of both reduction and oxidation processes from CV curves of tested compounds, CV measurements of the solutions of the compounds revealed bipolar behavior. **PyPhDMAC**, **PyPhPTZ**, and **PyPhPXZ** containing 9,9-dimethyl-10*H*-acridine, 9*H*-phenothiazine, and 9*H*-phenoxazine moieties, respectively, were characterized by the quasi-reversible oxidation process, while compound **PyPhCz** with 9*H*-carbazole fragment showed the irreversible oxidation waves during the first scan, probably due to the participation of unsubstituted C-3 and C-6 positions of 9*H*-carbazole.[32] The oxidation peaks of 2-pyridone derivatives were observed in the range of 0.28−0.88 V. Irreversible reduction processes with analogous shapes were observed for all of the studied compounds, due to the similar electron-deficient fragment. The reduction peaks were observed in the region of −2.52 to − 2.56 V. To estimate the IP$_{CV}$ and EA$_{CV}$ values, the onsets of oxidation and reduction potentials were used, respectively. The EA values were found to be quite similar for all of the investigated compounds (2.24−2.28 eV). The highest IP$_{CV}$ value of 5.68 eV was observed for the compound **PyPhCz** containing the 9*H*-carbazole fragment. The lower IP$_{CV}$ values (5.34, 5.12, and 5.08 eV) were obtained for other 2-pyridone-based derivatives. This observation can apparently be attributed to the stronger electron-donating effect of 9*H*-phenothiazine, 9*H*-phenoxazine, and 9,9-dimethyl-10*H*-acridane units.

Table 6. Electrochemical and Photoelectrical Characteristics of 2-Pyridone Derivatives[a]

compound	$E_{ox\ vs\ Fc^+/Fc}^{onset}$	$E_{red\ vs\ Fc^+/Fc}^{onset}$	IP$_{cv}$, eV	EA$_{CV}$, eV
PyPhCz	0.88	−2.53	5.68	2.27
PyPhDMAC	0.54	−2.52	5.34	2.28
PyPhPTZ	0.32	−2.55	5.12	2.25
PyPhPXZ	0.28	−2.56	5.08	2.24

[a]$E_{ox\ vs\ Fc^+/Fc}^{onset}$, $E_{red\ vs\ Fc^+/Fc}^{onset}$—onsets of oxidation and redaction potentials respectively; IP—ionization potential, IP$_{CV}$ = E_{ox}^{onset} + 4.8; EA—electron affinity, EA$_{CV}$ = 4.8 − |E_{red}^{onset}|.

2.5. Electroluminescent Properties. Taking into account the highest solid fluorescence quantum yield and TADF effect, we utilized compound **PyPhDMAC** for the fabrication of nondoped and exciplex emission-based OLEDs. The nondoped device **A** has the following structure:

https://doi.org/10.1021/acsaelm.3c00443
ACS Appl. Electron. Mater. 2023, 5, 4174−4186

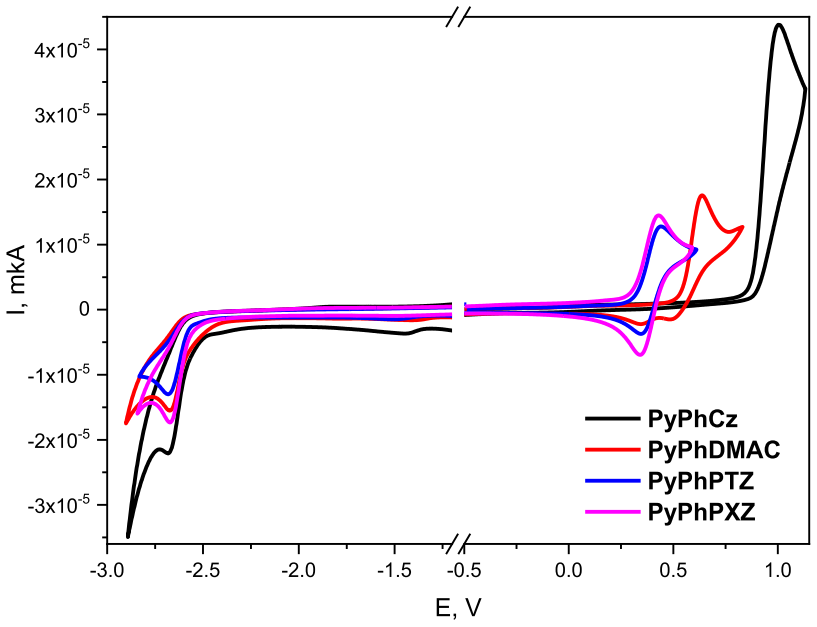

Figure 4. CV curves of the 2-pyridone-based derivatives.

Table 7. EL Characteristics of Devices A−C

device	V_{on}, V	brightness^{max}, Cd m^{-2}	η_c^{max}, cd A^{-1}	η_p^{max}, lm W^{-1}	EQE^{max}, %	λ_{max}^{EL}, nm	CIE$_{1976}$ (u,v)
A	6	9900	6.1	2.3	3.7	482	(0.134, 0.391)
B	5.8	31 200	15.7	6.5	6.9	517	(0.121, 0.478)
C	5.7	35 370	16.1	6.9	9.8	425/480/519	(0.151, 0.441)

V_{on}—torn-on voltage, η_c^{max}—maximum current efficiency, η_p^{max}—maximum power efficiency, EQE$_{max}$—maximum value of external quantum efficiency, λ_{max}^{EL}—EL maximum, CIE1$_{976}$ (u, v)—chromaticity coordinates.

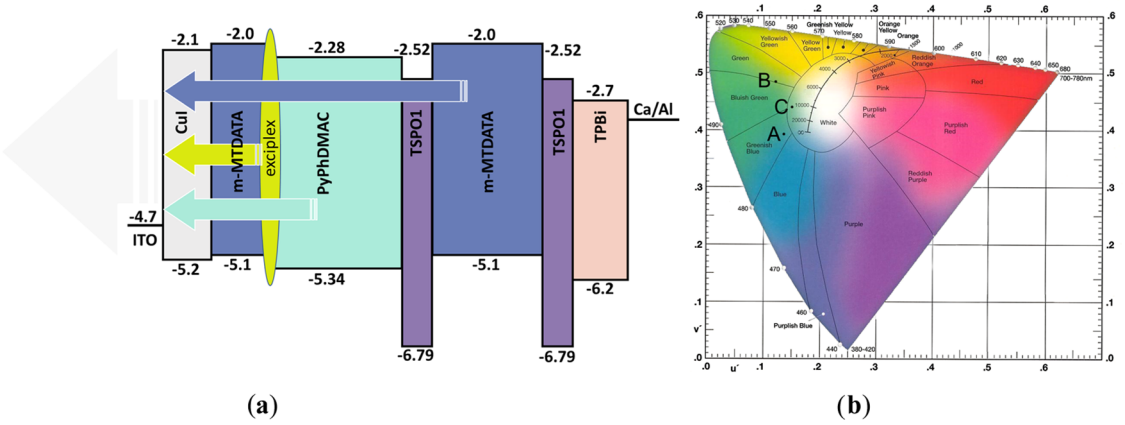

Figure 5. Schematic energy diagram of device **C** (a) and chromaticity diagram of devices **A−C** (b).

ITO/CuI(8 nm)/TPD(40 nm)/PyPhDMAC(20 mn)

/TSPO1(4 nm)/TPBi(40 nm)/Ca(50 nm)/Al(200 nm)

Devices **A−C** were fabricated by step-by-step deposition of hole- and electron transport layers, organic emissive layers, and metal electrodes onto precleaned ITO-coated glass substrate under a vacuum of 10^{-5} Torr. CuI[33] and TPD[34] (*N*,*N*′-bis(3-methylphenyl)-*N*,*N*′-diphenylbenzidine) were used as materials for hole-transporting layers. The TPBi[35] 2,2′,2″-(1,3,5-benzinetriyl)-tris(1-phenyl-1-H-benzimidazole) and TSPO1 (diphenyl-[4-(triphenylsilyl)phenyl]phosphine oxide)[36] were used as electron-transporting and hole-blocking layers, respectively. The hole transport layer (HTL) and the electron transport layer (ETL) were chosen to confine holes and electrons in the emitting layer that improves the performance of the device. The Ca layer topped with a 200 nm aluminum (Al) layer was used as the cathode.[37,38] The active area of the obtained devices was 2*3 mm^2. The density−voltage and luminance−voltage dependences were recorded using a semiconductor parameter analyzer HP4145A. Electroluminescence (EL) spectra were recorded with an Ocean Optics USB2000 spectrometer.

As shown in Figure S4, the emission maxima wavelengths of device **A** were located in the range of 440−480 nm, which was close to the PL spectrum of the solid film of **PyPhDMAC**. This observation confirms exciton recombination in the emitting layer. The EL spectra were stable in the wide range of driving

https://doi.org/10.1021/acsaelm.3c00443
ACS Appl. Electron. Mater. 2023, 5, 4174−4186

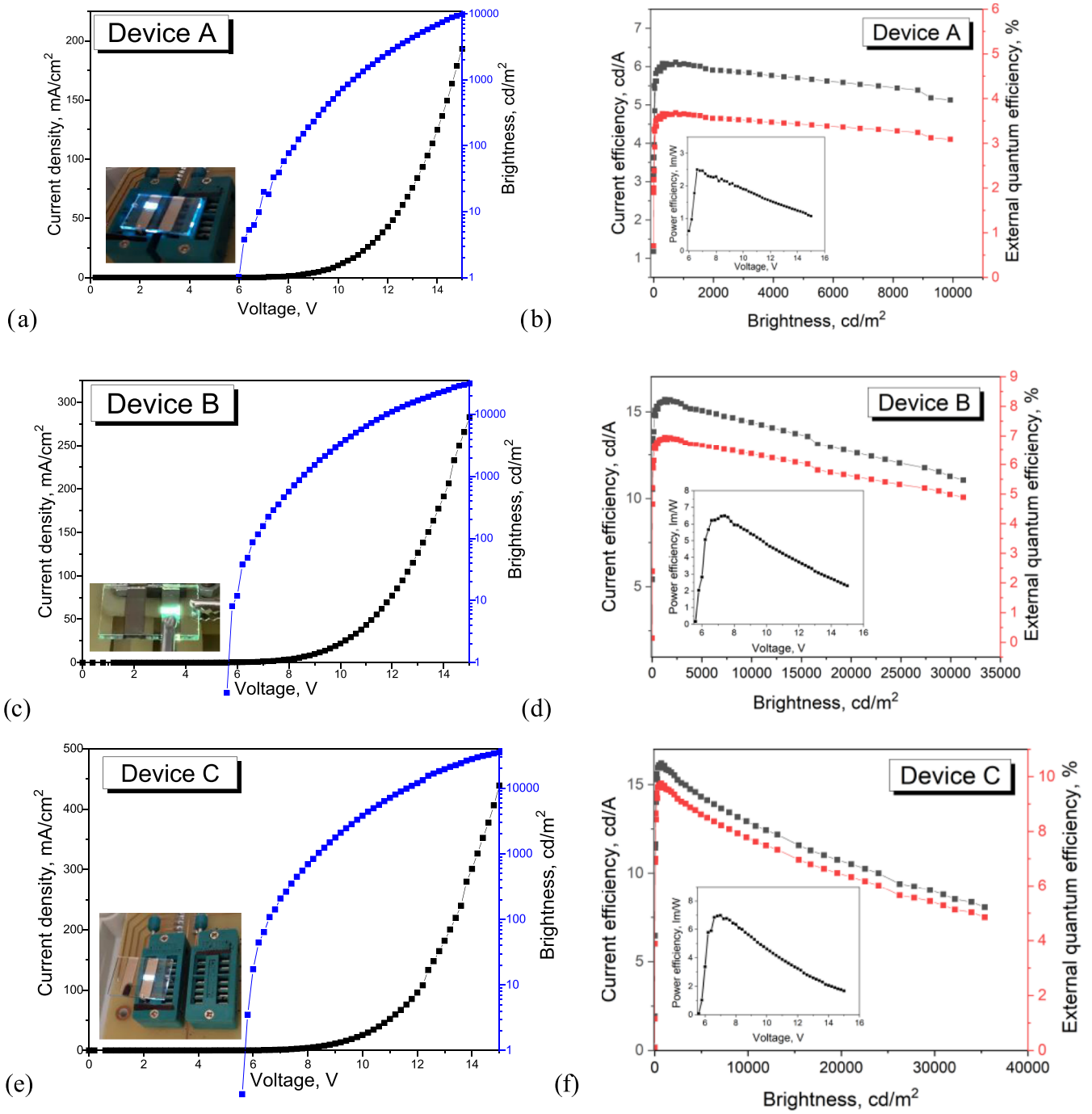

Figure 6. Current density and brightness versus voltage characteristics and photo of devices **A**−**C** (a, c, and e, respectively) and current efficiency-brightness-external quantum efficiency (b, d, and f, respectively) and power efficiency−voltage (inside) curves.

voltages, confirming the good color stability of the device (Figure S5a). Device **A** was characterized by relatively low-efficiency roll-off and good stability of efficiency of the device in all of the range of current density and by a maximum EQE value of 3.7% (Table 7).

The exciplex emission-based OLED was prepared taking into account the results of the investigation of the photophysical properties of the **PyPhDMAC**. The 4,4′,4″-tris[phenyl(*m*-tolyl)amino]triphenylamine (*m*-MTDATA) was used as the donor counterpart for **PyPhDMAC** to induce exciplex emission. The energy difference of the HOMOs of *m*-MTDATA and **PyPhDMAC** is 0.24 eV, while that for the LUMO levels is 0.28 eV (Figure 5a). The structure of device **B** was as follows:

ITO/CuI(8)/*m* - MTDATA(30 nm)/PyPhDMAC(30 nm)
/TSPO1(4 nm)/TPBi(40 nm)/Ca(50 nm)/Al(200 nm)

Figure S3b shows the relaxation dynamics of the exciplex emission of **PyPhDMAC** and *m*-MTDATA, which take longer times than the relaxation dynamics of fluorescence of solid films of **PyPhDMAC** or *m*-MTDATA. Because of the mismatch in the LUMO and HOMO energy levels, cross-coupling of the charge carriers occurred at the interface of the layers of *m*-MTDATA

https://doi.org/10.1021/acsaelm.3c00443
ACS Appl. Electron. Mater. 2023, 5, 4174−4186

and **PyPhDMAC** and as a result, intense broad exciplex emission was observed in the region of 500−750 nm (Figure S3a). The spectrum of the exciplex of the mixture of *m*-MTDATA and **PyPhDMAC** is broader and red-shifted in comparison to the spectra of the solid films of **PyPhDMAC** or *m*-MTDATA (Figure S3a).

In order to fabricate the efficient WOLED, the technique of combining basic colors was used. The three-color WOLED was realized by simultaneously combining the intrinsic emission and exciplex emissions of the same materials (Figure 5a) similarly to previously reported results.[39,40] The principal scheme of the fabricated WOLED based on exciplex enhanced TADF looks as follows:

ITO/CuI(8 nm)/*m* - MTDATA(20 nm)
/PyPhDMAC(40 nm)/TSPO1(4 nm)/*m* -
MTDATA(40 nm)/TSPO1(4 nm)/TPBi(40 nm)
/Ca(50 nm)/Al(200 nm)(device **C**)

Since **PyPhDMAC** exhibited good performance in nondoped sky-blue OLEDs, it was anticipated that using **PyPhDMAC** as the blue-emitting compound, high-performance white OLED (WOLED) can be obtained. To accomplish this goal, the efficient yellow-green exciplex emission was introduced into the device to design full-color WOLED. Additionally, the thin layer of *m*-MTDATA was used to get blue emission. The layers of **PyPhDMAC** and *m*-MTDATA were separated by the layer of TSPO1 in the device to disturb the injection of carriers. The second TSPO1 interlayer with a thickness of 4 nm could block energy transfer between *m*-MTDATA and TPBi and modify the recombination zone. As a result, the designed structure of the device **C** allowed us to obtain exciton recombination zones from three emitters, i.e., deep-blue *m*-MTDATA, sky-blue **PyPhDMAC**, and yellowish-green interface exciplex emitters. The resulting WOLED presented a combined emission from different excited states, i.e., blue emission from the layer of *m*-MTDATA thin layer, exciplex emission from the interface of the layer of *m*-MTDATA and **PyPhDMAC** and sky-blue exciton emission from **PyPhDMAC** (Figure 5b).

The lighting parameters are presented in Figures 6 and S6. Device **B**, based on exciplex emission of the interface of *m*-MTDATA and **PyPhDMAC** turned on at 5.8 V and showed high CE, PE, and EQE of 15.7 cd A^{-1}, 6.5 lm W^{-1}, and 6.9%, respectively (Table 7).

The graphs of the dependence of current efficiency and external quantum efficiency on brightness are shown in Figure 6. The external quantum efficiency was stable over the full scale of brightness and varied by 0.4% at luminance from 1000 to 10 000 Cd m^{-2}. For device **B**, the value of quantum efficiency dropped by 1.7%, and for device **C**, it was two times smaller at a brightness of 35 000 Cd m^{-2} compared to those at 100 Cd m^{-2}. On the one hand, these values are high for device **C**, but if we talk about operating voltages (1−10 V) and operating brightness (100−1000 Cd m^{-2}), the decrease in performance is also within 0.5−2%. On the other hand, in the present work, the performance parameters of devices at critical values of voltages and current densities were studied. In device C (Figures 6 and S8), the current density is very high at maximum brightness, which causes thermal degradation effects in the device. This is due to several reasons: the thickness of the device, energy barriers between the emissive and functional layers, and the presence of nonradiative transitions.

The WOLED (device **C**) based on the combination of three deep-blue, sky-blue, and green-yellow emitters with CIE coordinates (*u*, *v*) of 0.151; 0.441 showed a turn-on voltage of 5.7 V, EQE exceeding 9.8%, and CE of more than 16 Cd A^{-1}.

3. CONCLUSIONS

The new series of donor−acceptor compounds based on 2-pyridone were synthesized, and their properties were investigated experimentally and theoretically. It was determined that compounds containing 9*H*-carbazole or 9,9-dimethyl-9,10-dihydroacridine moiety are crystalline materials while derivatives of 2-pyridone with 9*H*-phenothiazine or 9*H*-phenoxazine fragment are capable to form amorphous layers. The compounds exhibit emission in the violet and blue regions. The derivative of 2-pyridone and 9-dimethyl-9,10-dihydroacridine is characterized by "hot" exciton TADF. Based on the theoretical calculations, it is assumed that a very large gap between T_2 and T_1 results in a slow internal conversion from T_2 to T_1. Therefore, the RISC process from T_2 to S_1 with a gap of only 0.01 eV is possible. Emissive TADF channel from T_2 to S_1 dominates over nonradiative quenching of "hot" excitons resulting in the external quantum efficiency of sky-blue OLED of 3.7%. The derivative containing a 9,9-dimethyl-9,10-dihydroacridine moiety also demonstrates exciplex-forming properties. The film of the compound and 4,4′,4″-tris[phenyl-(*m*-tolyl)amino]triphenylamine shows an exciplex emission at 520 nm. The studied 2-pyridone derivative was tested in exciplex-based OLEDs exhibiting green-yellow and white emissions. The best white emitting device showed maximum current efficiency of 16.1 cd A^{-1}, power efficiency of 16.9 lm W^{-1}, and external quantum efficiency of 9.8%.

4. EXPERIMENTAL SECTION

4.1. Instrumentation. ^{1}H and ^{13}C nuclear magnetic resonance (NMR) spectra were reordered on a Bruker DRX 400 P (400 MHz (^{1}H), 100 MHz (^{13}C)) spectrometer at room temperature in a deuterated chloroform ($CDCl_3$) solution. The data are given as chemical shifts in δ (ppm), and tetramethylsilane (TMS) was used as an internal standard. Mass spectra were obtained by the electrospray ionization mass spectrometry (ESI-MS) method on an Esquire-LC 00084 mass spectrometer. Elemental analysis was performed with EuroEA Elemental Analyzer.

UV/vis spectra were recorded in quartz cells on an AvaSpec-USB2 spectrophotometer for 10^{-5} M solutions of the compounds. Photoluminescence (PL) spectra of 10^{-5} M solutions of the compounds were performed on an Edinburgh Instruments' FLS980 fluorescence spectrometer. Thin solid films for recording UV/vis and PL spectra were prepared by spin-coating technique utilizing SPS-Europe Spin150 Spin processor using 2.5 mg/mL solutions of the compounds in THF on the precleaned quartz substrates. Photoluminescence quantum yields of the solutions and of the solid films were performed using the integrated sphere (Edinburgh Instruments) coupled to the FLS980 spectrometer, calibrated with two standards: quinine sulfate in 0.1 H_2SO_4 and rhodamine 6G in ethanol.[41] Fluorescence decay curves of the samples were measured using a time-correlated single photon counting technique utilizing the PicoQuant PDL 820 ps diode laser as an excitation source (wavelength of 374 nm).

Differential scanning calorimetry (DSC) measurements were made on a TA Instruments "DSC Q100" calorimeter. The samples were heated at a scan rate of 10 °C/min under a nitrogen atmosphere. Thermogravimetric analysis (TGA) was performed on a "Mettler TGA/SDTA851e/LF/1100" at a heating rate of 20 °C/min under a nitrogen atmosphere. Electrochemical measurements were done using μAutolab Type III (EcoChemie, Netherlands) potentiostat, in a three-electrode cell using platinum rod as the counter electrode, glassy carbon as the working electrode (diameter 2 mm), and $Ag/AgNO_3$ as the

https://doi.org/10.1021/acsaelm.3c00443
ACS Appl. Electron. Mater. 2023, 5, 4174−4186

reference electrode with a scan rate of 2.5 mV/s with concentration of compounds 1.0×10^{-4} mol/dm^3. The measurements were calibrated using internal standard ferrocene/ferrocenium (Fc/Fc^+). Cyclic voltammetry (CV) experiments were conducted in the dry solvent solution containing 0.1 M tetrabutylammonium hexafluorophosphate ($TBAPF_6$) as the electrolyte at room temperature under a nitrogen atmosphere. Deaeration of the solution was achieved by a nitrogen bubbling for ca. 10 min before measurement.

One of the synthesized derivatives was studied in electroluminescence devices. Devices were fabricated by vacuum deposition of organic semiconductor layers and metal electrodes onto the precleaned indium tin oxide (ITO)-coated glass substrate under vacuum of 10^{-6} Torr. ITO was used as the anode, which has great electric conductivity and light transmittance. Ca and Al are used as cathode. The HOMO energy level of CuI matches the structure with the weak potential barrier at the interface, which is conducive to hole injection and reducing the turn-on voltage, respectively. A hole-blocking layer (HBL) in the devices using TSPO1 is added between the emitting layer (*m*-MTDATA) and the electron-transporting layer, which blocks *m*-MTDATA and TPBi from forming exciplex at the interface. The density−voltage and luminance−voltage characteristics were measured by using a Keithley 6517 Binair instrument without passivation immediately after the preparation of the device. The brightness measurements were carried out by using a calibrated photodiode. The electroluminescence spectra were recorded with an Avaspec-2048L spectrometer. Device efficiencies were calculated from the luminance, current density, and EL spectrum.

4.2. Materials and Synthesis. The starting compounds, i.e., 2-hydroxypyridine, 1-bromo-4-iodobenzene, 9,10-dihydroacridine, 1,10-phenanthroline, palladium acetate ($Pd(CH_3COO)_2$), tri*tert*-butylphosphine ($P(t\text{-}Bu)_3$), copper, copper(I) chloride (CuCl), cesium carbonate (Cs_2CO_3), potassium carbonate (K_2CO_3), and sodium chloride (NaCl), were purchased from Sigma-Aldrich and used as received.

*4.2.1. 1-(4-Bromophenyl)pyridin-2(1H)-one (**BrPh2PY**).* BrPh2PY was synthesized by Ullmann condensation.[42] 1-Bromo-4-iodobenzene (7.45 g, 0.026 mol), 2-hydroxypyridine (2.5, 0.026 mol), copper (0.168 g, 2.6 mmol), copper(I) chloride (0.26 g, 2.6 mmol), potassium carbonate (7.26 g, 0.52 mol), and 1,10-phenanthroline (0.974 g, 3.4 mmol) were dissolved in dimethyl sulfoxide (DMSO) under argon atmosphere. The reaction mixture was heated at 140 °C for 24 h. After cooling, the reaction mixture was filtered through a 2 cm layer of Celite and washed with ethyl acetate. The solvent was removed under reduced pressure, and the product was recrystallized from isopropanol and vacuum-dried to afford light-brown crystals. ^{1}H NMR (400 MHz, $CDCl_3$) δ 7.55 (d, J = 8.3 Hz, 2H), 7.38−7.30 (m, 1H), 7.22 (t, J = 8.9 Hz, 3H), 6.62 (d, J = 9.3 Hz, 1H), 6.20 (t, J = 6.7 Hz, 1H). ^{13}C NMR (100 MHz, $CDCl_3$) δ: 162.21, 140.18, 139.78, 138.55, 137.50, 132.57, 128.33, 121.95, 106.44. Mp 100 °C.

*4.2.2. 1-(4-(9H-Carbazol-9-yl)phenyl)pyridin-2(1H)-one (**PyPhCz**).* **PyPhCz** was prepared by Ullmann condensation.[42] A mixture of BrPh2PY (0.5 g, 2.00 mmol), 9*H*-carbazole (0.4 g, 2.39 mmol), Cu (0.01 g, 0.20 mmol), CuCl (0.02 g, 0.20 mmol), K_2CO_3 (0.55 g, 3.98 mmol), and 1,10-phenanthroline (0.07 g, 0.40 mmol) were dissolved in *o*-DCB (10 mL) under an argon atmosphere. The reaction mixture was heated at 170 °C for 24 h. After cooling down, the reaction mixture was filtrated through a 2 cm layer of Celite and washed with dichloromethane (DCM). The solvent was removed under reduced pressure, and the crude product was purified by flash column chromatography on silica gel using an eluent system EtOAc/HEX = 1.5/1, crystallized from isopropanol and vacuum-dried to afford yellow crystals (0.58 g, 87% yield). ^{1}H NMR (400 MHz, $CDCl_3$) δ 8.08 (d, J = 7.8 Hz, 2H), 7.64 (d, J = 8.6 Hz, 2H), 7.57 (d, J = 8.6 Hz, 2H), 7.44−7.33 (m, 6H), 7.24 (t, J = 7.4 Hz, 2H), 6.65 (d, J = 8.9 Hz, 1H), 6.25 (t, J = 6.7 Hz, 1H). ^{13}C NMR (100 MHz, $CDCl_3$) δ: 162.40, 140.58, 140.08, 139.55, 137.82, 128.14, 127.67, 126.13, 123.59, 122.15, 120.36, 109.78, 106.32. Elemental analysis calcd for $C_{23}H_{16}N_2O$ (%): C 82.12, H 4.79, N 8.33, O 4.76; found (%): C 82.06, H 4.77, N 8.39. m/z: 336.13.

*4.2.3. 1-(4-(9,9-Dimethylacridin-10(9H)-yl)phenyl)pyridin-2(1H)-one (**PyPhDMAC**).* **PyPhDMAC** was prepared by the Buchwald−Hartwig cross-coupling reaction.[43] A mixture of appropriate BrPh2PY (0.5 g, 2.00 mmol), 9,9-dimethyl-10*H*-acridane (0.5 g, 2.39 mmol), and Cs_2CO_3 (1.30 g, 4.00 mmol) was dissolved under argon in dry toluene (10 mL) and was stirred for 10 min at room temperature. Then, $Pd(CH_3COO)_2$ (0.09 g, 0.40 mmol) and $P(t\text{-}Bu)_3$ (0.04 g, 0.19 mmol) under argon were added. The reaction mixture was heated at 100 °C for 24 h. After cooling down, the reaction mixture was filtrated through a 2 cm layer of Celite and washed with DCM. After that, the solvent was removed under reduced pressure. The crude product was purified by flash column chromatography on silica gel using eluent system EtOAc/HEX = 1.5/1, crystallized from isopropanol, and vacuum-dried to afford olive crystals (0.33 g, 45% yield). ^{1}H NMR (400 MHz, $CDCl_3$) δ 7.61 (d, J = 8.5 Hz, 2H), 7.45−7.34 (m, 6H), 6.96−6.84 (m, 4H), 6.65 (d, J = 9.2 Hz, 1H), 6.25 (dd, J = 11.0, 7.4 Hz, 3H), 1.62 (s, 6H). ^{13}C NMR (100 MHz, $CDCl_3$) δ: 162.29, 141.29, 140.60, 140.05, 137.79, 132.29, 130.14, 129.08, 126.45, 125.31, 122.18, 120.84, 114.17, 106.27, 35.99, 31.25. Elemental analysis calcd for $C_{26}H_{22}N_2O$ (%): C 82.51, H 5.86, N 7.40, O 4.23; found (%): C 82.46, H 5.91, N 7.45. m/z: 378.17.

*4.2.4. 1-(4-(10H-Phenothiazin-10-yl)phenyl)pyridin-2(1H)-one (**PyPhPTZ**).* **PyPhPTZ** was prepared by the same method as **PyPhDMAC**, starting from BrPh2PY (0.5 g, 2.00 mmol), phenothiazine (0.29 g, 2.44 mmol), Cs_2CO_3 (1.30 g, 4.00 mmol), Pd(CH3COO)$_2$ (0.09 g, 0.40 mmol), and $P(t\text{-}Bu)_3$ (0.04 g, 0.19 mmol) in dry toluene (10 mL). The crude product was purified by flash column chromatography on silica gel using an eluent system EtOAc/HEX = 1.5/1, crystallized from isopropanol, and vacuum-dried to afford white crystals (0.31 g, 43% yield). ^{1}H NMR (400 MHz, $CDCl_3$) δ 7.51 (d, J = 8.6 Hz, 2H), 7.39 (d, J = 8.7 Hz, 2H), 7.37−7.33 (m, 2H), 7.03 (dd, J = 7.4, 1.4 Hz, 2H), 6.85 (dt, J = 24.7, 7.2 Hz, 4H), 6.65−6.60 (m, 1H), 6.39 (d, J = 8.0 Hz, 2H), 6.22 (t, J = 6.7 Hz, 1H). ^{13}C NMR (100 MHz, $CDCl_3$) δ: 162.33, 140.02, 139.46, 137.78, 129.34, 128.66, 127.09, 123.29, 122.63, 122.11, 117.97, 106.25. Elemental analysis calcd for $C_{23}H_{16}N_2OS$ (%): C 74.98, H 4.38, N 7.60, O 4.34, S 8.70; found (%): C 74.92, H 4.33, N 7.66, S 8.75. m/z: 368.10.

*4.2.5. 1-(4-(10H-Phenoxazin-10-yl)phenyl)pyridin-2(1H)-one (**PyPhPXZ**).* **PyPhPXZ** was prepared by the same method as **PyPhDMAC**, starting from BrPh2PY (0.5 g, 2.00 mmol), phenoxazine (0.44 g, 2.40 mmol), Cs_2CO_3 (1.30 g, 4.00 mmol), $Pd(CH_3COO)_2$ (0.09 g, 0.40 mmol), and $P(t\text{-}Bu)_3$ (0.04 g, 0.19 mmol) in dry toluene (10 mL). The crude product was purified by flash column chromatography on silica gel using eluent system EtOAc/HEX = 1.5/1, crystallized from isopropanol, and vacuum-dried to afford light-brown crystals (0.31 g, 45% yield). ^{1}H NMR (400 MHz, $CDCl_3$) δ 7.57 (d, J = 8.5 Hz, 2H), 7.44−7.33 (4H), 6.66−6.52 (m, 8H), 5.94 (dd, J = 7.8, 1.3 Hz, 2H). ^{13}C NMR (100 MHz, $CDCl_3$) 162.23, 143.94, 140.70, 140.10, 139.08, 137.62, 134.00, 131.86, 129.29, 123.31, 122.17, 121.66, 115.58, 113.44, 106.35. Elemental analysis calcd for $C_{23}H_{16}N_2O_2$ (%): C 78.39, H 4.58, N 7.95, O 9.08; found (%): C 78.44, H 4.04, N 7.89. m/z: 352.12.

4.3. Computational Details. Ground singlet state (S_0) of **PyPhCz**, **PyPhDMAC**, **PyPhPTZ**, and **PyPhPXZ** molecules were optimized at the B3LYP/6-31G(d)[44−47] level of density functional theory (DFT) using Grimme's empirical dispersion correction (GD3).[48] Based on optimized S_0 state geometries, the first singlet excited state (S_1) geometry was optimized by time-dependent (TD) DFT method[49] employing the same GD3-B3LYP/6-31G(d) approach, while the first triplet excited state (T_1) was optimized by spin-unrestricted UB3LYP/6-31G(d) method. The polarizable continuum model (PCM) was used during all geometry optimization procedures.[50] By using optimized S_1 and T_1 geometries, the energies of singlet and triplet excited states were clarified by range-separated LC-ωPBE[51] with manually tuned ω value equal to 0.14 that gives the best agreement with experimentally observed fluorescence wavelength. All of these calculations were performed within Gaussian16 software.[52] The spin−orbit coupling matrix elements $\langle S_1|\hat{\mathbf{H}}_{SO}|T_n\rangle$ were calculated by using zeroth-order regular approximation (ZORA)[53] for $\hat{\mathbf{H}}_{SO}$ operator at TDDFT/PBE0/TZP[54,55] level of theory with accounting of solvent effect within COSMO model[56] similarly to the methodology proposed by Brédas et al.[57] SOC calculations were performed within ADF2021 software.[58]

https://doi.org/10.1021/acsaelm.3c00443
ACS Appl. Electron. Mater. 2023, 5, 4174−4186

■ ASSOCIATED CONTENT

Supporting Information

The Supporting Information is available free of charge at https://pubs.acs.org/doi/10.1021/acsaelm.3c00443.

Thermal properties (DSC curves), photophysical properties of the studied materials and electroluminescence properties of the fabricated devices, and ^{1}H and ^{13}C spectra of synthesized materials (PDF)

■ AUTHOR INFORMATION

Corresponding Authors

Glib V. Baryshnikov − *Laboratory of Organic Electronics, Department of Science and Technology, Linköping University, SE-60174 Norrköping, Sweden; Department of Chemistry and Nanomaterials Science, Bohdan Khmelnytsky National University, 18031 Cherkasy, Ukraine;* orcid.org/0000-0002-0716-3385; Email: glib.baryshnikov@liu.se

Juozas V. Grazulevicius − *Department of Polymer Chemistry and Technology, Kaunas University of Technology, Kaunas 51423, Lithuania;* orcid.org/0000-0002-4408-9727; Email: juozas.grazulevicius@ktu.lt

Authors

Iryna Danyliv − *Lviv Polytechnic National University, 79013 Lviv, Ukraine*

Khrystyna Ivaniuk − *Lviv Polytechnic National University, 79013 Lviv, Ukraine*

Yan Danyliv − *Lviv Polytechnic National University, 79013 Lviv, Ukraine;* orcid.org/0000-0001-9645-0337

Igor Helzhynskyy − *Lviv Polytechnic National University, 79013 Lviv, Ukraine*

Viktorija Andruleviciene − *Department of Polymer Chemistry and Technology, Kaunas University of Technology, Kaunas 51423, Lithuania*

Dmytro Volyniuk − *Department of Polymer Chemistry and Technology, Kaunas University of Technology, Kaunas 51423, Lithuania;* orcid.org/0000-0003-3526-2679

Pavlo Stakhira − *Lviv Polytechnic National University, 79013 Lviv, Ukraine*

Complete contact information is available at: https://pubs.acs.org/10.1021/acsaelm.3c00443

Notes

The authors declare no competing financial interest.

■ ACKNOWLEDGMENTS

This work was supported by the Ministry of Education and Science of Ukraine (project nos. 0123U101690 and 0121U107533). The quantum-chemical calculations were performed with computational resources provided by National Academic Infrastructure for Supercomputing in Sweden (NAISS 2023/5-77) at the National Supercomputer Centre (NSC) at Linköping University partially funded by the Swedish Research Council through grant agreement no. 2022-06725. G.B. thanks the support by the Swedish Research Council through starting grant no. 2020-04600. This project also received funding from European Social Fund (project no. 09.3.3-LMT-K-712-23-0125) under grant agreement with the Research Council of Lithuania (LMTLT).

■ REFERENCES

(1) Fröbel, M.; Fries, F.; Schwab, T.; Lenk, S.; Leo, K.; Gather, M. C.; Reineke, S. Three-Terminal RGB Full-Color OLED Pixels for Ultrahigh Density Displays. *Sci. Rep.* **2018**, *8*, No. 9684.

(2) Yi, C. H. Core OLED Technology Could Change the Display Landscape. *Inf. Disp.* **2023**, *39* (1), 27−31.

(3) Choi, S.; Kwon, S.; Kim, H.; Kim, W.; Kwon, J. H.; Lim, M. S.; Lee, H. S.; Choi, K. C. Highly Flexible and Efficient Fabric-Based Organic Light-Emitting Devices for Clothing-Shaped Wearable Displays. *Sci. Rep.* **2017**, *7*, No. 6424.

(4) Uoyama, H.; Goushi, K.; Shizu, K.; Nomura, H.; Adachi, C. Highly Efficient Organic Light-Emitting Diodes from Delayed Fluorescence. *Nature* **2012**, *492* (7428), 234−238.

(5) Dias, F. B.; Bourdakos, K. N.; Jankus, V.; Moss, K. C.; Kamtekar, K. T.; Bhalla, V.; Santos, J.; Bryce, M. R.; Monkman, A. P. Triplet Harvesting with 100% Efficiency by Way of Thermally Activated Delayed Fluorescence in Charge Transfer OLED Emitters. *Adv. Mater.* **2013**, *25* (27), 3707−3714.

(6) Santos, P. L.; Ward, J. S.; Data, P.; Batsanov, A. S.; Bryce, M. R.; Dias, F. B.; Monkman, A. P. Engineering the Singlet−Triplet Energy Splitting in a TADF Molecule. *J. Mater. Chem. C* **2016**, *4* (17), 3815−3824.

(7) Tao, Y.; Yuan, K.; Chen, T.; Xu, P.; Li, H.; Chen, R.; Zheng, C.; Zhang, L.; Huang, W. Thermally Activated Delayed Fluorescence Materials Towards the Breakthrough of Organoelectronics. *Adv. Mater.* **2014**, *26* (47), 7931−7958.

(8) Zhang, Q.; Li, J.; Shizu, K.; Huang, S.; Hirata, S.; Miyazaki, H.; Adachi, C. Design of Efficient Thermally Activated Delayed Fluorescence Materials for Pure Blue Organic Light Emitting Diodes. *J. Am. Chem. Soc.* **2012**, *134* (36), 14706−14709.

(9) Xu, Y.; Xu, P.; Hu, D.; Ma, Y. Recent Progress in Hot Exciton Materials for Organic Light-Emitting Diodes. *Chem. Soc. Rev.* **2021**, *50* (2), 1030−1069.

(10) Xu, Y.; Liang, X.; Zhou, X.; Yuan, P.; Zhou, J.; Wang, C.; Li, B.; Hu, D.; Qiao, X.; Jiang, X.; Liu, L.; Su, S. J.; Ma, D.; Ma, Y. Highly efficient blue fluorescent OLEDs based on upper level triplet-singlet intersystem crossing. *Adv. Mater.* **2019**, *31* (12), No. 1807388.

(11) Xu, Y.; Xu, P.; Hu, D.; Ma, Y. Recent progress in hot exciton materials for organic light-emitting diodes. *Chem. Soc. Rev.* **2021**, *50*, 1030−1069.

(12) Lv, X.; Xu, L.; Yu, Y.; Cui, W.; Zhou, H.; Cang, M.; Sun, Q.; Pan, Y.; Xue, S.; Yang, W. High external quantum efficiency and low efficiency roll-off achieved simultaneously in nondoped pure-blue organic light-emitting diodes based on a hot-exciton fluorescent material. *Chem. Eng. J.* **2021**, *408*, No. 127333.

(13) Tsiko, U.; Volyniuk, D.; Andruleviciene, V.; Leitonas, K.; Sych, G.; Bezvikonnyi, O.; Jasinskas, V.; Gulbinas, V.; Stakhira, P.; Grazulevicius, J. V. Triphenylamino or 9-phenyl carbazolyl-substituted pyrimidine-5-carbonitriles as bipolar emitters and hosts with triplet harvesting abilities. *Mater. Today Chem.* **2022**, *25*, No. 100955.

(14) Rajamalli, P.; Senthilkumar, N.; Huang, P. Y.; Ren-Wu, C. C.; Lin, H. W.; Cheng, C. H. New Molecular Design Concurrently Providing Superior Pure Blue, Thermally Activated Delayed Fluorescence and Optical Out-Coupling Efficiencies. *J. Am. Chem. Soc.* **2017**, *139* (32), 10948−10951.

(15) Liang, X.; Tu, Z. L.; Zheng, Y. X. Thermally Activated Delayed Fluorescence Materials: Towards Realization of High Efficiency through Strategic Small Molecular Design. *Chem. − Eur. J.* **2019**, *25* (22), 5623−5642.

(16) Mei, Y.; Liu, D.; Li, J.; Wang, J. Thermally Activated Delayed Fluorescence Materials Based on Acridin-9(10H)-One Acceptor for Organic Light-Emitting Diodes. *Dyes Pigm.* **2022**, *207*, No. 110701.

(17) Nagamura, N.; Sasabe, H.; Sato, H.; Kamata, T.; Ito, N.; Araki, S.; Abe, S.; Sukegawa, Y.; Yokoyama, D.; Kaji, H.; Kido, J. A Multifunctional Hole-Transporter for High-Performance TADF OLEDs and Clarification of Factors Governing the Transport Property by Multiscale Simulation. *J. Mater. Chem. C* **2022**, *10* (22), 8694−8701.

(18) Lee, H.; Park, J. H.; Yang, K. J.; Hwang, S. J.; Braveenth, R.; Ha, T. H.; Han, M. I.; Lee, C. W.; Kwon, J. H. CN-Substituted Ortho-

Terphenyl Core Based High Triplet Energy Bipolar Host Materials for Stable and Efficient Blue TADF Devices. *J. Mater. Chem. C* **2021**, *9* (23), 7426−7435.
(19) Rodella, F.; Bagnich, S.; Duda, E.; Meier, T.; Kahle, J.; Athanasopoulos, S.; Köhler, A.; Strohriegl, P. High Triplet Energy Host Materials for Blue TADF OLEDs—A Tool Box Approach. *Front. Chem.* **2020**, *8*, 657.
(20) Cho, Y. J.; Jeon, S. K.; Lee, J. Y. Molecular Engineering of High Efficiency and Long Lifetime Blue Thermally Activated Delayed Fluorescent Emitters for Vacuum and Solution Processed Organic Light-Emitting Diodes. *Adv. Opt. Mater.* **2016**, *4* (5), 688−693.
(21) Lee, D. R.; Kim, B. S.; Lee, C. W.; Im, Y.; Yook, K. S.; Hwang, S. H.; Lee, J. Y. Above 30% External Quantum Efficiency in Green Delayed Fluorescent Organic Light-Emitting Diodes. *ACS Appl. Mater. Interfaces* **2015**, *7* (18), 9625−9629.
(22) Cha, J. R.; Lee, C. W.; Lee, J. Y.; Gong, M. S. Design of Ortho-Linkage Carbazole-Triazine Structure for High-Efficiency Blue Thermally Activated Delayed Fluorescent Emitters. *Dyes Pigm.* **2016**, *134*, 562−568.
(23) Xiang, Y.; Gong, S.; Zhao, Y.; Yin, X.; Luo, J.; Wu, K.; Lu, Z. H.; Yang, C. Asymmetric-Triazine-Cored Triads as Thermally Activated Delayed Fluorescence Emitters for High-Efficiency Yellow OLEDs with Slow Efficiency Roll-Off. *J. Mater. Chem. C* **2016**, *4* (42), 9998−10004.
(24) Wu, K.; Zhang, T.; Zhan, L.; Zhong, C.; Gong, S.; Jiang, N.; Lu, Z. H.; Yang, C. Optimizing Optoelectronic Properties of Pyrimidine-Based TADF Emitters by Changing the Substituent for Organic Light-Emitting Diodes with External Quantum Efficiency Close to 25% and Slow Efficiency Roll-Off. *Chem. − Eur. J.* **2016**, *22* (31), 10860−10866.
(25) Pan, K. C.; Li, S. W.; Ho, Y. Y.; Shiu, Y. J.; Tsai, W. L.; Jiao, M.; Lee, W. K.; Wu, C. C.; Chung, C. L.; Chatterjee, T.; Li, Y. S.; Wong, K. T.; Hu, H. C.; Chen, C. C.; Lee, M. T. Efficient and Tunable Thermally Activated Delayed Fluorescence Emitters Having Orientation-Adjustable CN-Substituted Pyridine and Pyrimidine Acceptor Units. *Adv. Funct. Mater.* **2016**, *26* (42), 7560−7571.
(26) Liu, W.; Zheng, C. J.; Wang, K.; Chen, Z.; Chen, D. Y.; Li, F.; Ou, X. M.; Dong, Y. P.; Zhang, X. H. Novel Carbazol-Pyridine-Carbonitrile Derivative as Excellent Blue Thermally Activated Delayed Fluorescence Emitter for Highly Efficient Organic Light-Emitting Devices. *ACS. Appl. Mater. Interfaces* **2015**, *7* (34), 18930−18936.
(27) Bomzon, B.; Khunger, Y.; Subramanian, R. A Dielectric and Spectrophotometric Study of the Tautomerization of 2-Hydroxypyridine and 2-Mercaptopyridine in Water. *RSC Adv.* **2020**, *10* (4), 2389−2395.
(28) Cui, L. S.; Gillett, A. J.; Zhang, S. F.; Ye, H.; Liu, Y.; Chen, X.-K.; Lin, Z.-S.; Evans, E. W.; Myers, W. K.; Ronson, T. K.; Nakanotani, H.; Reineke, S.; Bredas, J.-L.; Adachi, C.; Friend, R. H. Fast spin-flip enables efficient and stable organic electroluminescence from charge-transfer states. *Nat. Photonics* **2020**, *14*, 636−642.
(29) Etherington, M. K.; Gibson, J.; Higginbotham, H. F.; Penfold, T. J.; Monkman, A. P. Revealing the Spin−Vibronic Coupling Mechanism of Thermally Activated Delayed Fluorescence. *Nat. Commun.* **2016**, *7*, No. 13680.
(30) Samanta, P. K.; Kim, D.; Coropceanu, V.; Brédas, J. L. Up-Conversion Intersystem Crossing Rates in Organic Emitters for Thermally Activated Delayed Fluorescence: Impact of the Nature of Singlet vs Triplet Excited States. *J. Am. Chem. Soc.* **2017**, *139* (11), 4042−4051.
(31) Schleper, A. L.; Goushi, K.; Bannwarth, C.; Haehnle, B.; Welscher, P. J.; Adachi, C.; Kuehne, A. J. C. Hot Exciplexes in U-Shaped TADF Molecules with Emission from Locally Excited States. *Nat. Commun.* **2021**, *12*, No. 6179.
(32) Chiu, S.-K.; Chung, Y.-C.; Liou, G.-S.; Su, Y. O. Electrochemical and Spectral Characterizations of 9-Phenylcarbazoles. *J. Chin. Chem. Soc.* **2012**, *59* (3), 331−337.
(33) Stakhira, P.; Cherpak, V.; Volynyuk, D.; Ivastchyshyn, F.; Hotra, Z.; V Tataryn, V.; Luka, G. Characteristics of organic light emitting diodes with copper iodide as injection layer. *Thin Solid Films* **2010**, *518*, 7016−7018.
(34) Yamashita, K.; Mori, T.; Mizutani, T.; Miyazaki, H.; Takeda, T. EL properties of organic light-emitting-diode using TPD derivatives with diphenylstylyl groups as hole transport layer. *Thin Solid Films* **2000**, *363* (1−2), 33−36.
(35) Wang, J.; Liu, J.; Huang, S.; Wu, X.; Shi, X.; Chen, C.; Ye, Z.; Lu, J.; Su, Y.; He, G.; Zheng, Y. High efficiency green phosphorescent organic light-emitting diodes with a low roll-off at high brightness. *Org. Electron.* **2013**, *14*, 2854−2858.
(36) Mamada, M.; Ergun, S.; Pérez-Bolívar, C.; Anzenbacher, P., Jr. Charge transport, carrier balance, and blue electrophosphorescence in diphenyl [4-(triphenylsilyl)phenyl] phosphine oxide devices. *Appl. Phys. Lett.* **2011**, *98* (7), No. 073305.
(37) Feng, X. D.; Khangura, R.; Lu, Z. H. Metal−organic−metal cathode for high-contrast organic light-emitting diodes. *Appl. Phys. Lett.* **2004**, *85* (3), 497−499.
(38) Smith, L. H.; Wasey, J. A. E.; Barnes, W. L. Light outcoupling efficiency of top-emitting organic light-emitting diodes. *Appl. Phys. Lett.* **2004**, *84* (16), 2986−2988.
(39) Wang, G.; Yin, M.; Miao, Y.; Guo, Y.; Zhou, H.; Lu, Q.; Huang, J.; Wang, H. Combining intrinsic (blue) and exciplex (green and orange-red) emissions of the same material (OCT) in white organic light-emitting diodes to realize high color quality with a CRI of 97. *J. Mater. Chem. C* **2022**, *10*, 6654−6664.
(40) Grybauskaite-Kaminskiene, G.; Ivaniuk, K.; Bagdziunas, G.; Turyk, P.; Stakhira, P.; Baryshnikov, G.; Volyniuk, D.; Cherpak, V.; Minaev, B.; Hotra, Z.; Ågren, H.; Grazulevicius, J. V. Contribution of TADF and exciplex emission for efficient "warm-white" OLEDs. *J. Mater. Chem. C* **2018**, *6*, 1543−1550.
(41) de Mello, J. C.; Wittmann, H. F.; Friend, R. H. An improved experimental determination of external photoluminescence quantum efficiency. *Adv. Mater.* **1997**, *9*, 230−232.
(42) Weingarten, H. Mechanism of the Ullmann condensation1. *J. Org. Chem.* **1964**, *29* (12), 3624−3626.
(43) Li, J. J. *Name Reactions*; Springer: Berlin Heidelberg, 2009.
(44) Becke, A. D. Density-functional thermochemistry. III. The role of exact exchange. *J. Chem. Phys.* **1993**, *98*, 5648−5652.
(45) Lee, C.; Yang, W.; Parr, R. G. Development of the Colle-Salvetti correlation-energy formula into a functional of the electron density. *Phys. Rev. B* **1988**, *37*, 785−789.
(46) Ditchfield, R.; Hehre, W. J.; People, J. A. Self-Consistent Molecular-Orbital Methods. IX. An Extended Gaussian-Type Basis for Molecular-Orbital Studies of Organic Molecules. *J. Chem. Phys.* **1971**, *54*, 724.
(47) Frisch, M. J.; Pople, J. A.; People, J. A. Self-consistent molecular orbital methods 25. Supplementary functions for Gaussian basis sets. *J. Chem. Phys.* **1984**, *80*, 3265−3269.
(48) Grimme, S.; Antony, J.; Ehrlich, S.; Krieg, H. A consistent and accurate ab initio parametrization of density functional dispersion correction (DFT-D) for the 94 elements H-Pu. *J. Chem. Phys.* **2010**, *132*, No. 154104.
(49) Casida, M. E.; Jamorski, C.; Casida, K. C.; Salahub, D. R. Molecular excitation energies to high-lying bound states from time-dependent density-functional response theory: Characterization and correction of the time-dependent local density approximation ionization threshold. *J. Chem. Phys.* **1998**, *108*, 4439.
(50) Tomasi, J.; Mennucci, B.; Cammi, R. Quantum Mechanical Continuum Solvation Models. *Chem. Rev.* **2005**, *105* (8), 2999−3094.
(51) Vydrov, O. A.; Scuseria, G. E. Assessment of a long-range corrected hybrid functional. *J. Chem. Phys.* **2006**, *125*, No. 234109.
(52) Frisch, M. J.; Trucks, G. W.; Schlegel, H. B.; Scuseria, G. E.; Robb, M. A.; Cheeseman, J. R.; Scalmani, G.; Barone, V.; Petersson, G. A.; Nakatsuji, H.; Li, X.; Caricato, M.; Marenich, A. V.; Bloino, J.; Janesko, B. G.; Gomperts, R.; Mennucci, B.; Hratchian, H. P.; Ortiz, J. V.; Izmaylov, A. F.; Sonnenberg, J. L.; Williams-Young, D.; Ding, F.; Lipparini, F.; Egidi, F.; Goings, J.; Peng, B.; Petrone, A.; Henderson, T.; Ranasinghe, D.; Zakrzewski, V. G.; Gao, J.; Rega, N.; Zheng, G.; Liang, W.; Hada, M.; Ehara, M.; Toyota, K.; Fukuda, R.; Hasegawa, J.; Ishida, M.; Nakajima, T.; Honda, Y.; Kitao, O.; Nakai, H.; Vreven, T.; Throssell, K.; Montgomery, J. A., Jr.; Peralta, J. E.; Ogliaro, F.; Bearpark,

https://doi.org/10.1021/acsaelm.3c00443
ACS Appl. Electron. Mater. 2023, 5, 4174−4186

M. J.; Heyd, J. J.; Brothers, E. N.; Kudin, K. N.; Staroverov, V. N.; Keith, T. A.; Kobayashi, R.; Normand, J.; Raghavachari, K.; Rendell, A. P.; Burant, J. C.; Iyengar, S. S.; Tomasi, J.; Cossi, M.; Millam, J. M.; Klene, M.; Adamo, C.; Cammi, R.; Ochterski, J. W.; Martin, R. L.; Morokuma, K.; Farkas, O.; Foresman, J. B.; Fox, D. J. *Gaussian 16, Revision B.01*; Gaussian, Inc.: Wallingford CT, 2016.

(53) Van Lenthe, E.; Ehlers, A.; Baerends, E.-J. Geometry optimizations in the zero order regular approximation for relativistic effects. *J. Chem. Phys.* **1999**, *110*, 8943.

(54) Ernzerhof, M.; Scuseria, G. E. Assessment of the Perdew−Burke−Ernzerhof exchange-correlation functional. *J. Chem. Phys.* **1999**, *110*, 5029.

(55) Van Lenthe, E.; Baerends, E. J. Optimized Slater-type basis sets for the elements 1−118. *J. Comput. Chem.* **2003**, *24* (9), 1142−1156.

(56) Klamt, A.; Schüürmann, G. COSMO: a new approach to dielectric screening in solvents with explicit expressions for the screening energy and its gradient. *J. Chem. Soc. Perkin Trans. 2* **1993**, 799−805.

(57) Samanta, P. K.; Kim, D.; Coropceanu, V.; Brédas, J.-L. Up-Conversion Intersystem Crossing Rates in Organic Emitters for Thermally Activated Delayed Fluorescence: Impact of the Nature of Singlet vs Triplet Excited States. *J. Am. Chem. Soc.* **2017**, *139* (11), 4042−4051.

(58) te Velde, G.; Bickelhaupt, F. M.; Baerends, E. J.; Fonseca Guerra, C.; van Gisbergen, S. J. A.; Snijders, J. G.; Ziegler, T. Chemistry with ADF. *J. Comput. Chem.* **2001**, *22* (9), 931−967.

Recommended by ACS

Suppression of Dexter Energy Transfer through Modulating Donor Segments of Thermally Activated Delayed Fluorescence Assistant Dopants

Jihyun Lee, Jun Yeob Lee, *et al.*

APRIL 19, 2023
ACS APPLIED MATERIALS & INTERFACES

READ

Highly Efficient Triplet–Triplet Annihilation Upconversion with a Thermally Activated Delayed Fluorescence Molecule as Triplet Photosensitizer

Min Zheng, Xiaoguo Zhou, *et al.*

FEBRUARY 03, 2023
THE JOURNAL OF PHYSICAL CHEMISTRY C

READ

Impact of Electron-Donating Groups on Attaining Dual-Emitting Imidazole-Based Donor–Acceptor Materials

Prabhu Ganesan, Peng Gao, *et al.*

MARCH 15, 2023
THE JOURNAL OF ORGANIC CHEMISTRY

READ

Efficient Nondoped Pure Red/Near-Infrared TADF OLEDs by Designing and Adjusting Double Quantum Wells Structure

Yufu Sun, Liang Zhou, *et al.*

JUNE 30, 2022
ACS APPLIED ELECTRONIC MATERIALS

READ

Get More Suggestions >

https://doi.org/10.1021/acsaelm.3c00443
ACS Appl. Electron. Mater. 2023, 5, 4174−4186